

CHEMISTRY

AN ASIAN JOURNAL

www.chemasianj.org

Accepted Article

Title: Multiply fused anthracenes as helical polycyclic aromatic hydrocarbon motif for chiroptical performance enhancement

Authors: Kei Fujise, Eiji Tsurumaki, Gaku Fukuhara, Nobuyuki Hara, Yoshitane Imai, and Shinji Toyota

This manuscript has been accepted after peer review and appears as an Accepted Article online prior to editing, proofing, and formal publication of the final Version of Record (VoR). This work is currently citable by using the Digital Object Identifier (DOI) given below. The VoR will be published online in Early View as soon as possible and may be different to this Accepted Article as a result of editing. Readers should obtain the VoR from the journal website shown below when it is published to ensure accuracy of information. The authors are responsible for the content of this Accepted Article.

To be cited as: *Chem. Asian J.* 10.1002/asia.202000394

Link to VoR: <https://doi.org/10.1002/asia.202000394>

A Journal of



A sister journal of *Angewandte Chemie*
and *Chemistry – A European Journal*

WILEY-VCH

COMMUNICATION

Multiply fused anthracenes as helical polycyclic aromatic hydrocarbon motif for chiroptical performance enhancement

Kei Fujise,^[a] Eiji Tsurumaki,^[a] Gaku Fukuhara,^[a,b] Nobuyuki Hara,^[c] Yoshitane Imai,^[c] Shinji Toyota*^[a]

[a] K. Fujise, Dr. E. Tsurumaki, Prof. Dr. G. Fukuhara, Prof. Dr. S. Toyota
Department of Chemistry, School of Science
Tokyo Institute of Technology
2-12-1 Ookayama, Meguro-ku, Tokyo 152-8551 (Japan)
E-mail: stoyota@chem.titech.ac.jp

[b] Prof. Dr. G. Fukuhara
JST, PRESTO
4-1-8 Honcho, Kawaguchi, Saitama, 332-0012 (Japan)

[c] N. Hara, Prof. Dr. Y. Imai
Department of Applied Chemistry, Faculty of Science and Engineering
Kindai University
3-4-1 Kowakae, Higashi-Osaka, Osaka 577-8502 (Japan)

Supporting information and the ORCID identification numbers for the authors of this article can be found via a link at the end of the document.

Polycyclic aromatic hydrocarbons consisting of three fused anthracene units were designed as new π -conjugated compounds having helical structures. These expanded helicenes were synthesized by Pt-catalyzed cycloisomerization of the corresponding ethynyl-substituted precursors. The nonplanar and helical structure was confirmed by X-ray analysis and DFT calculations, and the barrier to helical inversion was estimated to be 34 kJ mol⁻¹. The enantiomers of the diphenyl derivative were successfully resolved by chiral HPLC. Enantiopure samples showed good chiroptical performance in the CD ($[\Delta\epsilon]$ 1380 L mol⁻¹ cm⁻¹) and CPL ($[g]_{lum}$ 0.013) spectra, and these values were considerably large for simple organic molecules. The unique chiroptical properties are discussed on the basis of the molecular structure and the electronic state with the aid of time-dependent DFT calculations.

Helicenes are the most fundamental motif for designing helical chiral molecules from angularly fused benzene units.^[1] A large number of enantiopure helicenes and related compounds having remarkable chiroptical properties, namely, optical rotation, circular dichroism (CD), and circularly polarized luminescence (CPL), were synthesized as nonplanar π -conjugated compounds.^[2] Their characteristic properties and functions owing to the helical π systems have led to several applications in the fields of material science, supramolecular chemistry, and so on.^[3] In order to construct novel structures, the fundamental helicene structure ([6]helicene: **1**) has been modified in several ways, including the lengthening of the helical chain^[4] and the introduction of multiple helical sites.^[5] Another way to enlarge the helical structure is the insertion of a linearly fused benzene ring into angularly fused units (Figure 1): such compounds are called "expanded helicenes" according to the classification by Tilley et al., who synthesized compound **2** by intramolecular cycloaddition.^[6,7] In 2018, Hirose and Matsuda et al. reported expanded helicene **3** as a helical analog of kekulene, in which five benzene rings are inserted.^[8] However, the chiroptical properties of these expanded helicenes were not well investigated because

of the facile racemization (calculated barrier 54 kJ mol⁻¹) via helical inversion. In this study, we designed compound **4** consisting of three fused anthracene units as a new type of π -conjugated expanded helicene, in which three benzene rings are inserted into the structure of **1**. The presence of three anthracene substructures in **4** would give novel properties as chromophore and fluorophores.^[9,10] We herein report the synthesis, structures, and photophysical properties of new expanded helicene **4**. We resolved the enantiomers of a phenyl-substituted derivative, which showed excellent chiroptical performance in the CD and CPL spectra compared with other helical hydrocarbons and simple organic molecules. Because CPL-active compounds have recently attracted attention as chiral organic devices,^[11] we discuss these novel properties of the anthracene system with the aid of density functional theory (DFT) calculations.

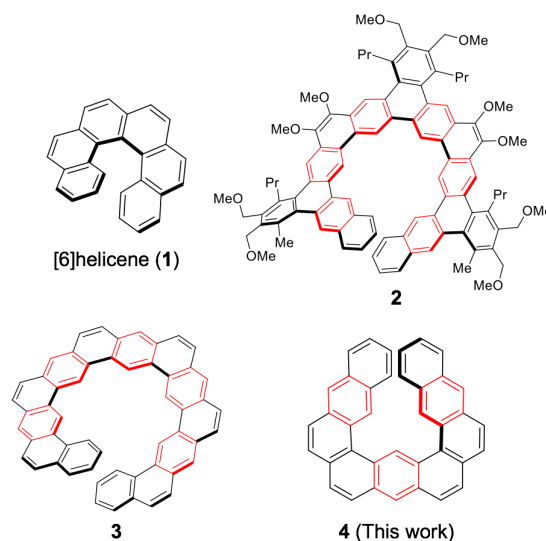
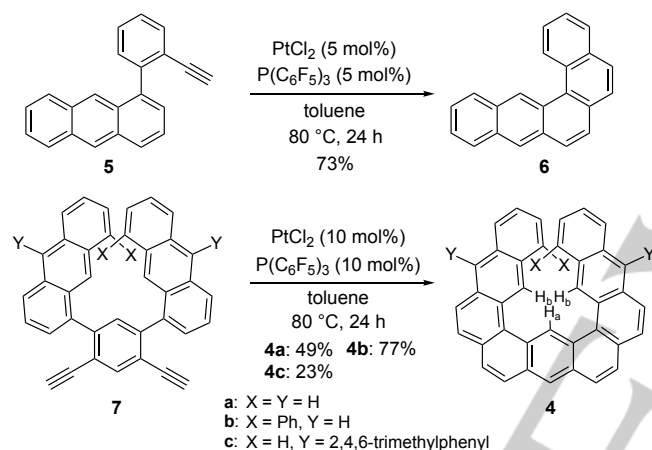


Figure 1. Structures of [6]helicene (**1**) and its expanded analogs **2–4**. Inserted linearly fused benzene rings are highlighted in red.

COMMUNICATION

The fused anthracene system was constructed by the cycloisomerization reaction of 1-(2-ethynylphenyl)anthracene derivatives because this reaction was occasionally utilized for the synthesis of phenanthrene derivatives from 2-ethynyl-1,1'-biphenyl derivatives via the 6-*endo* cyclization reaction.^[12] The reaction conditions were optimized for the PtCl₂-catalyzed cycloisomerization of **5** as the model reaction (Scheme 1 and Table S1). When **5** was heated in toluene in the presence of P(C₆F₅)₃ ligand,^[13] naphtho[1,2-*a*]anthracene (**6**) was obtained in 73% yield without the formation of a significant amount of other cyclized products. Compound **7a** was similarly reacted to give doubly cyclized product **4a** in 49% yield as a yellow solid. Phenyl-substituted derivative **4b** and 2,4,6-trimethylphenyl (mesityl) substituted derivative **4c** were similarly synthesized from the corresponding precursors.^[14] Compound **4a**, dianthra[1,2-*a*:2',1'-*j*]anthracene, which consists of three fused anthracene units, is a new aromatic ring parent. These products were characterized by their NMR and mass spectra, and their structures were confirmed by X-ray analysis as mentioned below.



Scheme 1. Synthesis of **6** and **4** by PtCl₂-catalyzed cycloisomerization.

In the ¹H NMR spectrum of **4a**, the signal due to H_a in the central anthracene unit was observed at 12.11 ppm as a singlet. The unusual deshielding of the proton in the cove area was attributed to the strong ring current effects of the surrounding aromatic moieties as well as the steric compression effect.^[15] In fact, an intense nuclear Overhauser effect (41%) was observed for the H_a signal upon irradiation of the H_b signal (Figure S1), and

this value was close to the theoretical maximum (50%) for homonuclear coupling.^[16] For **4b**, restricted rotation of the phenyl groups was observed by variable-temperature ¹H NMR measurements (Figure S3). The barrier determined by the dynamic NMR method ($\Delta G^{\ddagger}_{298} = 53 \text{ kJ mol}^{-1}$) was lower than that of the enantiomerization mentioned later. This value of **4b** is comparable to the calculated rotational barrier of the phenyl group in 1-phenylanthracene ($\Delta G^{\ddagger}_{298} = 55 \text{ kJ mol}^{-1}$).^[17]

The UV-vis and fluorescence spectra of **4a** and **4b** were measured in CHCl₃ (Figure S7 and Table 1). Compound **4a** gave an intense peak at 346 nm and a series of absorption bands extending to 470 nm, which were bathochromically shifted by 50–80 nm relative to those of anthracene and [6]helicene.^[18] The absorption at the longest wavelength (λ_{max} 459 nm) was assigned to the HOMO→LUMO transition according to the time-dependent (TD)-DFT calculation mentioned later. In the fluorescence spectrum, **4a** showed an intense emission band at 467 nm (Φ 0.18, τ 9.6 ns). Its fluorescence quantum yield was much larger than that of [6]helicene (Φ 0.03), which underwent intersystem crossing rapidly at the excited state,^[19] as revealed by the increased fluorescence emission rate constant k_f and the slightly decreased nonradiative decay rate constant k_{nr} . The small Stokes shift of **4a** (370 cm⁻¹) demonstrated that the structural change at the excited state should be small. These bathochromic effects in the absorption and emission spectra indicated that the π -conjugation was effectively extended by the fused anthracene units in **4a**. Compound **4b** having phenyl groups showed similar absorption and emission spectra with bathochromic shifts by 4–6 nm relative to **4a**.

The X-ray structures of **4a** are shown in Figure 2(a). The molecule had a helical structure to avoid steric hindrance between the terminal benzene rings. As a result, the interatomic distance C(1)⋯C(19) (3.99 Å) was larger than the sum of their van der Waals radii (3.40 Å). The torsion angles along the inner carbons were ca. 10° for one [4]helicene moiety and ca. 20° for the other, meaning that the two moieties had different torsional curves. The angle between the mean planes of the terminal benzene rings (A and I) was 30.2°, and this value was smaller than the corresponding angle (59.5°) in [6]helicene^[20] and larger than those in **2** (6.3°)^[6] and **3** (18.2°).^[8] The interatomic distances between the H_a and H_b atoms (1.88 and 1.78 Å) were much smaller than the sum of the van der Waals radii (2.40 Å), being consistent with the NMR data mentioned above. This helical structure of **4a** was nearly reproduced by DFT calculations at the M06-2X/6-31G(d,p) level (Figure S25). The optimized structure was ideally C₂ symmetric and the dihedral angles along the inner carbons in the [4]helicene region were 12.4° or 22.4°. The packing

Table 1. UV-vis and fluorescence spectral data of **4a**, **4b**, anthracene, and [6]helicene (**1**).^[a]

	UV-vis	FL					Stokes shift
	λ_{max} [nm] (ϵ [L mol ⁻¹ cm ⁻¹])	λ_{em} [nm]	Φ [b]	τ [ns] [c]	k_f [ns ⁻¹] [d]	k_{nr} [ns ⁻¹] [e]	[cm ⁻¹]
4a	459 (2900), 346 (56300), 287 (105000)	467	0.18	9.6	0.019	0.086	370
<i>rac</i> - 4b	465 (3000), 352 (56600), 298 (71900)	471	0.15	8.5	0.018	0.10	270
anthracene	379 (9000)	383	0.12	2.0	0.060	0.44	280
1 [f]	410 (250)	420	0.03	8.4	0.0036	0.12	580

[a] Measured in CHCl₃ at room temperature unless otherwise noted. [b] Absolute fluorescence quantum yield. [c] Fluorescence lifetime. [d] Fluorescence emission rate constant: $k_f = \Phi/\tau$. [e] Nonradiative decay rate constant: $k_{nr} = (1-\Phi)/\tau$. [f] Ref. 18. Measured in CH₂Cl₂.

COMMUNICATION

diagram in Figure 2(b) showed that molecules of the same helicity were stacked linearly via $\pi \cdots \pi$ interactions along the *b* axis, which extended to the long axis of a needle-like single crystal. In the X-ray structure of **4a**, the bond alternation was significant for benzene rings C, D, F, and G as parameterized by the HOMA index (Table S3).^[21] The C(6)–C(7), C(8)–C(9), C(11)–C(12), and C(13)–C(14) bonds were shorter than the other bonds, and had high double-bond character. The NICS(0) values were calculated for each benzene ring in the optimized structure at the GIAO-B3LYP/6-31G(d,p) level: A(I) –9.55, B(H) –11.52, C(G) –5.32, D(F) –6.47, and E –11.57.^[22] These experimental and theoretical data indicated that the aromatic character was high for the linearly fused benzene rings and low for the angularly fused benzene rings, as illustrated in Clar's structure in Figure 2(c).

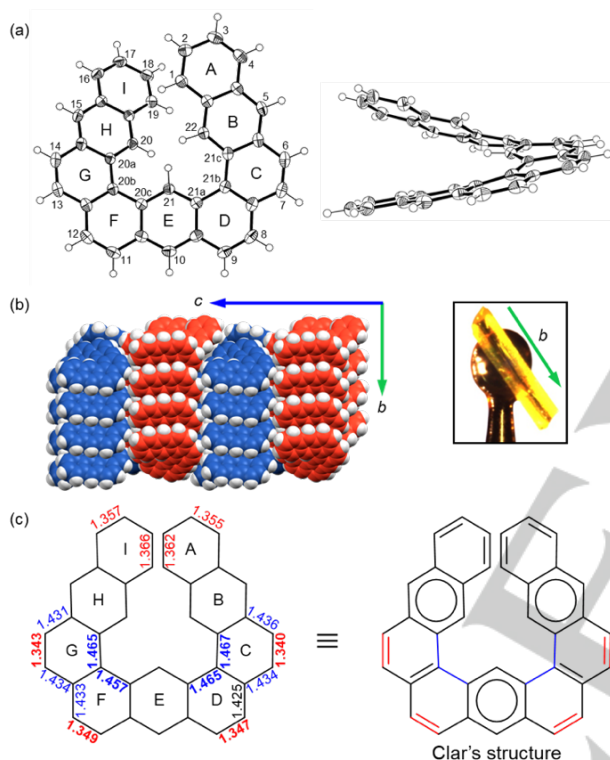


Figure 2. X-ray structures of **4a**. (a) Two views of ORTEP drawing with thermal ellipsoids at 50% probability. Dihedral angles: C(20)–C(20a)–C(20b)–C(20c) 19.4°, C(20a)–C(20b)–C(20c)–C(21) 19.7°, C(21)–C(21a)–C(21b)–C(21c) 9.5°, C(21a)–C(21b)–C(21c)–C(22) 11.1°. Interatomic distances: H(20)⋯H(21) 1.88 Å, H(21)⋯H(22) 1.78 Å, C(1)⋯C(19) 3.99 Å. Interplanar angle: plane(A)–plane(I) 30.2°. (b) Packing diagram and a picture of the single crystal measured. Red and blue models show *P* and *M* molecules, respectively. (c) Selected C–C bond distances in Å. Blue and red values indicate long and short bonds, respectively, relative to the normal aromatic bond.

Although the helical inversion in **4a** resulted in enantiomerization of the chiral compound, this compound lacked a probe to observe this dynamic process by NMR spectroscopy. Therefore, we measured the NMR spectra of the mesityl derivative **4c**, in which the two *o*-Me groups should be nonequivalent in the fixed helical structure (Figure 3a).^[23] Because the rotation of the mesityl groups relative to the aromatic framework was highly restricted,^[23] the site exchange between the Me_A and Me_B should occur by enantiomerization via the helical inversion. The signal due to the *o*-Me groups was measured as a

singlet at room temperature and even at –90 °C in CD₂Cl₂ (Figure S6). This observation meant that the enantiomerization occurred much faster than the NMR time scale (barrier <35 kJ mol^{–1}). The DFT calculation revealed that the enantiomerization of global minimum structure X proceeded in three steps via intermediate Y and its enantiomer (Figure 3b). The calculated barrier to helical inversion, namely the energy difference between X and TS2 (C_s symmetric butterfly structure), was 25.2 kJ mol^{–1} at 298 K, and this value is consistent with the above NMR observation. This barrier was much lower than that of [6]helicene (151 kJ mol^{–1}),^[24] and lower than those of expanded helicenes **2** and **3** (45–55 kJ mol^{–1}) in Figure 1.^[6,8]

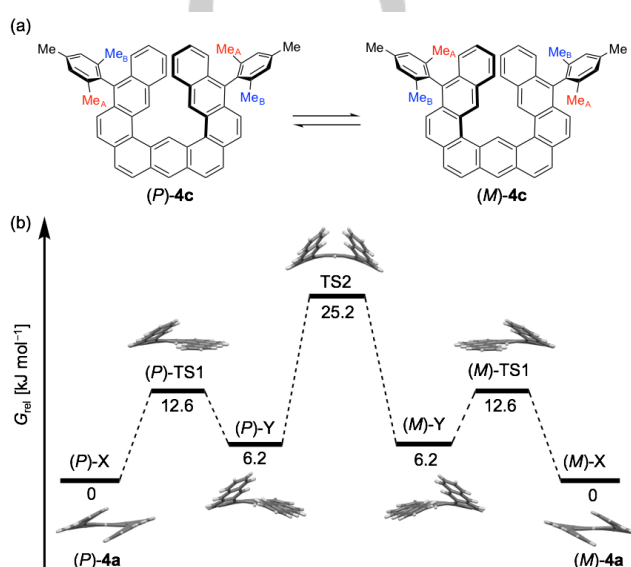


Figure 3. Enantiomerization via helical inversion of **4**. (a) Site exchange of *o*-Me groups in 2,4,6-trimethylphenyl groups in **4c**. (b) Mechanism of helical inversion of **4a** calculated at M06-2X/6-31G(d,p) level.

The calculated barrier to enantiomerization of **4a** was too low to isolate enantiomers at room temperature. However, the enantiomers of diphenyl derivative **4b** were successfully resolved by chiral HPLC with a Daicel CHIRALPAK-IC column (Figure S20). The first and second eluted fractions showed negative and positive Cotton effects, respectively, at 352 nm in the CD spectra. Each enantiomer slowly racemized on heating at 90 °C in toluene, and kinetic analysis gave barrier to enantiomerization $\Delta G^{\ddagger}_{363}$ of 121 kJ mol^{–1}. Because this barrier was much higher than the estimated value of **4a**, the phenyl groups effectively enhanced the barrier to helical inversion by destabilization of the transition state. The X-ray structures of **4b** (Figures S15 and S16) showed that the helical pitch [C(1)⋯C(19) 5.74 Å] was increased by the steric effects of the phenyl groups.

In order to examine the chiroptical properties of **4b**, we measured the CD and CPL spectra of enantiopure samples in CHCl₃ at room temperature. As clearly shown in Figure 4, the spectra of the enantiomers were mirror images of each other. In the CD spectrum, the second fraction gave a large positive Cotton effect at 352 nm ($\Delta\epsilon +1380$, $g_{\text{abs}} +0.024$) and a large negative Cotton effect at 297 nm ($\Delta\epsilon -1020$, $g_{\text{abs}} -0.014$) in addition to a weak one at 465 nm ($\Delta\epsilon -44$, $g_{\text{abs}} -0.015$), in which g_{abs} is absorption dissymmetry factor defined by $\Delta\epsilon/\epsilon$. The magnitude of the molar CD $|\Delta\epsilon|$ rarely exceeded 1000 for small organic

COMMUNICATION

molecules, and the value of **4b** at 352 nm was larger than those of a double-[6]helicene (801)^[18] and a nanographene propeller (1182)^[25] as well as [6]helicene (284).^[18] This characteristic property is consistent with the general tendency that increased twisting in aromatic moieties increase the Cotton effect.^[26] We calculated the CD spectrum of (*P*)-**4b** by the TDDFT method at the B3LYP/6-31G(d,p) level (Figure S31). The shapes and signs of the calculated bands agreed with the experimental spectrum of the second eluted isomer. Therefore, we were able to determine the absolute stereochemistry of **4b** as (*P*)-[CD(+)]352 or (*M*)-[CD(-)]352. This assignment was also supported by the X-ray analysis of the [CD(-)]352 isomer, in which the Flack parameter was nearly zero (0.028) on refinement of the *M* structure.^[27]

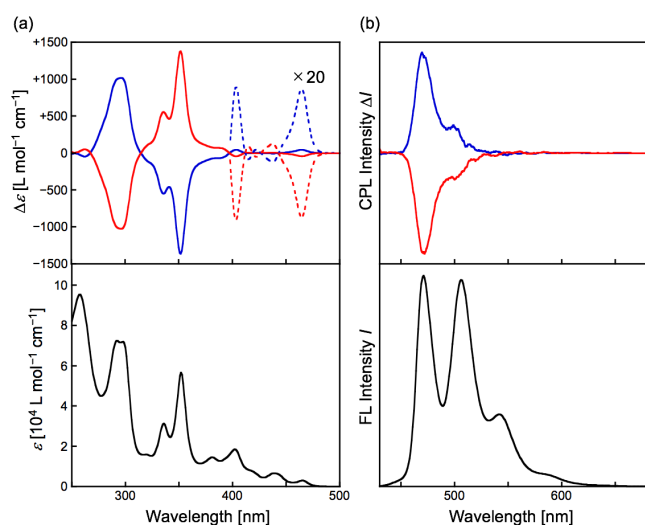


Figure 4. Chiroptical data of enantiopure **4b** in CHCl₃ at room temperature. (a) CD and UV-vis spectra. (b) CPL and FL spectra. Blue line: first fraction, (*M*)-**4b**. Red line: second fraction, (*P*)-**4b**.

The enantiomers of **4b** were CPL-active; (*M*)- and (*P*)-**4b** gave positive and negative bands, respectively, at 471 nm (Figure 4b). Luminescence dissymmetry factor g_{lum} , which is defined by the relative difference between left- and right-circularly polarized

emission,^[2a] was +0.013 and -0.012 for (*M*)- and (*P*)-**4b**, respectively. In general, non-aggregated small organic molecules exhibit only small $|g_{lum}|$ values of 10⁻⁵ to 10⁻³ order, if CPL-active, and examples of the values in the 10⁻² order are limited.^[11,28] As for carbohelicenes, typical reported values were 0.0009 for [6]helicene,^[18] 0.0025 for double-[6]helicene,^[18] 0.032 for bitriphenylene-type helicene.^[29] Therefore, compound **4b** featured a very large $|g_{lum}|$ value with retention of emissive property.

To obtain further information about the optical and chiroptical properties, we carried out TDDFT calculations of **4a** at the B3LYP/6-31G(d,p)//M06-2X/6-31G(d,p) level as the model of **4b** (Figure 5).^[30] The HOMO-LUMO gap of **4a** (2.97 eV) was smaller than that of [6]helicene (4.03 eV) as a result of the extended π -conjugation in the former. The observed absorption at 459 nm of **4a** was attributed to the HOMO→LUMO excitation. The calculated data of the electric (μ) and magnetic (m) transition dipole moments for important transitions in (*P*)-**4a** are compiled in Table 3. The two transition dipole moments determined the CD and CPL intensities according to the following equations: rotatory strength $R = |\mu||m|\cos\theta$ and $g = 4|\mu||m|\cos\theta/(|\mu|^2+|m|^2) \approx 4|m|\cos\theta/|\mu|$, where θ is the angle between them.^[31] The transition dipole moments for the symmetry-conserved $S_0 \rightarrow S_1$ transition in the C_2 symmetric structure of (*P*)-**4a** were antiparallel ($\theta = 180^\circ$), maximizing the magnitude of the angle term in R and g values.^[2c] In contrast, the two dipole moments were nonparallel ($\theta = 68^\circ$) for the transition at 353 nm ($S_0 \rightarrow S_7$), during which the orbital symmetry was not conserved. Nevertheless, the ratio $|m|/|\mu|$ was so large that the g value (+0.0196) was still large. This value was 1.8 times larger than that of the corresponding transition of (*P*)-[6]helicene **1** ($S_0 \rightarrow S_3$) (Table S8). The magnitude of the g value was further enhanced to +0.0313 by the introduction of the two phenyl substituents in (*P*)-**4b** (Table S7). This situation produced the strong Cotton effect at 356 nm for enantiopure **4b**. Table 3 also shows the transition dipole moments in the excited state ($S_1 \rightarrow S_0$), which corresponds to the emission at 471 nm. For the same reason as above, the dipole moments were antiparallel to enhance the $|g_{lum}|$ value (0.0043). This feature contrasted that of [6]helicene, in which the two transition dipole moments were nearly orthogonal, leading to very small $|g_{lum}|$ ($S_1 \rightarrow S_0$) as well as $|g_{abs}|$ value ($S_0 \rightarrow S_1$) values (Table S8). Thus, the intense CD and CPL bands were reasonably explained by the magnitudes and angles of the two transition dipole moments. This feature is

Table 2. Chiroptical properties of (*P*)-**4b**, (*M*)-**4b**, and (*P*)-[6]helicene (**1**).^[a]

	CD				FL	
	λ [nm]	$\Delta\epsilon$ [L mol ⁻¹ cm ⁻¹]	ϵ [L mol ⁻¹ cm ⁻¹] ^[b]	g_{abs} ^[c]	λ_{em} [nm]	g_{lum} ^[d]
<i>(P)</i> - 4b	465	-44	3000	-0.015	472	-0.012
	352	+1380	56600	+0.024		
	297	-1020	71800	-0.014		
<i>(M)</i> - 4b	465	+43	3000	+0.015	469	+0.013
	352	-1370	56600	-0.024		
	297	+1020	71800	+0.014		
<i>(P)</i> - 1 ^[e]	410	-0.3	250	-0.0012	420	-0.0009
	325	+284	27000	+0.0092		

[a] Measured in CHCl₃ at room temperature unless otherwise noted. [b] For (*P*)-**4b** and (*M*)-**4b**, molar absorption coefficients at peaks or troughs in the CD spectra, read from the UV-vis spectrum of *rac*-**4b**. [c] Absorption dissymmetry factor, $g_{abs} = \Delta\epsilon/\epsilon$. [d] Luminescence dissymmetry factor. [e] Ref 18. Measured in CH₂Cl₂.

COMMUNICATION

attributed to the anthracene based chromophores in the helical system.

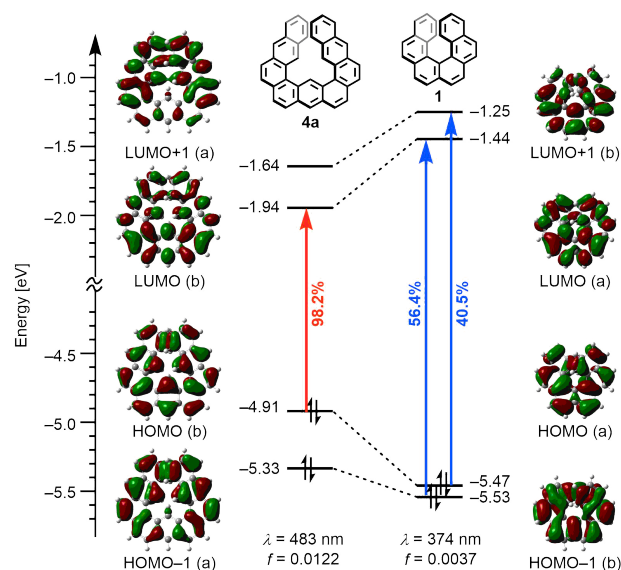


Figure 5. Frontier Kohn-Sham orbitals and orbital energy diagrams of **4a** and [6]helicene (**1**) calculated at the TD-B3LYP/6-31G(d,p)//M06-2X/6-31G(d,p) level. Data of the transition of the lowest energy are shown. λ : transition energy, f : oscillator strength.

Table 3. Transition dipole moments for selected transitions of (*P*)-**4a** calculated at the TD-B3LYP/6-31G(d,p)//M06-2X/6-31G(d,p) level.

Transition	$S_0 \rightarrow S_1$	$S_0 \rightarrow S_7$	$S_1 \rightarrow S_0$
λ [nm] ^[a]	482	353	541
$ \mu $ ^[b]	111.78	423.79	144.90
$ m $ ^[c]	0.1587	5.4702	0.1559
$\cos \theta$ ^[d]	-1.000	0.380	-1.000
g ^[e]	-0.0057	+0.0196	-0.0043
Orientation of μ and m			

[a] Transition energy. [b] Magnitude of electric transition dipole moment in 10^{-20} esu cm units. [c] Magnitude of magnetic transition dipole moment in 10^{-20} erg G^{-1} units. [d] θ : angle between the electric and magnetic transition dipole moments. [e] Dissymmetry factor, $g = 4|\mu||m| \cos \theta / (|\mu|^2 + |m|^2)$. g_{abs} for absorption and g_{lum} for luminescence.

In summary, expanded helicenes **4** consisting of three fused anthracene units were synthesized by the Pt-catalyzed cycloisomerization of alkynes. X-ray analysis and DFT calculations revealed that substituent-free compound **4a** had a helical structure that underwent helical inversion rapidly at room temperature. The enantiomers of diphenyl derivative **4b** were resolved by chiral HPLC and exhibited very intense Cotton effects in the CD spectra and very large magnitudes of g_{lum} factors in the CPL spectra for simple organic compounds. The TDDFT

calculations indicated that the magnitudes and directions of the electric and magnetic transition dipole moments in **4** were in good balance to enhance the chiroptical performance, in contrast to [6]helicene. These results demonstrate the critical role of the structural expansion of helicenes in their chiroptical properties, which would pave the way for designing novel advanced chiral molecules and materials, in particular circularly polarized devices. Further studies of synthesis of the further fused or expanded anthracene compounds as well as the properties and functions of these π -conjugated compounds are in progress.

Acknowledgements

This work was partly supported by JSPS KAKENHI Grant Number JP20H02721 and Nagase Science and Technology Foundation. The authors thank Professor Osamu Ishitani and Dr. Yusuke Tamaki for the measurements of fluorescence spectra, Professor Ken Ohmori and Professor Keisuke Suzuki for the use of a chiral HPLC system, and Professor Kan Wakamatsu for the valuable discussion on the theoretical calculations.

Conflict of interest

The authors declare no conflict of interest.

Keywords: arenes • circular dichroism • circularly polarized luminescence • density functional calculations • helical structures

- [1] a) C.-F. Chen, Y. Shen, *Helicene Chemistry: From Synthesis to Applications*, Springer, Berlin, **2017**; b) Y. Shen, C.-F. Chen, *Chem. Rev.* **2012**, *112*, 1463–1535. (c) M. Gingras, *Chem. Soc. Rev.* **2013**, *42*, 968–1006.
- [2] a) Y. Nakai, T. Mori, Y. Inoue, *J. Phys. Chem. A* **2013**, *117*, 83–93; b) I. Warnke, F. Furche, *WIREs Comput. Mol. Sci.* **2012**, *2*, 150–166; c) F. Furche, R. Ahlrichs, C. Wachsmann, E. Weber, I. H. Delgado, J. Lacour, R. Naaman, S. Grimme, *J. Am. Chem. Soc.* **2000**, *122*, 1717–1724.
- [3] a) T. Verbiest, S. V. Elshocht, M. Kauranen, L. Hellemans, J. Snauwaert, C. Nuckolls, T. J. Katz, A. Persoons, *Science* **1998**, *282*, 913–915; b) V. Kiran, S. P. Mathew, S. R. Cohen, I. H. Delgado, J. Lacour, R. Naaman, *Adv. Mater.* **2016**, *28*, 1957–1962; c) Y. Yang, R. C. da Costa, M. J. Fuchter, A. J. Campbell, *Nat. Photonics* **2013**, *7*, 634–638; d) M. Gingras, *Chem. Soc. Rev.* **2013**, *42*, 1051–1095.
- [4] a) P. Sehnal, I. G. Stará, D. Šaman, M. Tichý, J. Mišek, J. Cvačka, L. Rulíšek, J. Chocholoušová, J. Vacek, G. Goryl, M. Szymonski, I. Cisařová, I. Starý, *Proc. Nat. Acad. Sci. USA* **2009**, *106*, 13169–13174; b) K. Mori, T. Murase, M. Fujita, *Angew. Chem. Int. Ed.* **2015**, *54*, 6847–6851; *Angew. Chem.* **2015**, *127*, 6951–6955.
- [5] a) C. Li, Y. Yang, Q. Miao, *Chem. Asian J.* **2018**, *13*, 884–894; b) K. Kato, Y. Segawa, K. Itami, *Synlett* **2019**, *30*, 370–377; c) T. Hosokawa, Y. Takahashi, T. Matsushima, S. Watanabe, S. Kikkawa, I. Azumaya, A. Tsurusaki, K. Kamikawa, *J. Am. Chem. Soc.* **2017**, *139*, 18512–18521; d) V. Bereznaia, M. Roy, N. Vanthuyne, M. Villa, J.-V. Naubron, J. Rodriguez, Y. Coquerel, M. Gingras, *J. Am. Chem. Soc.* **2017**, *139*, 18508–18511; e) Y. Wang, Z. Yin, Y. Zhu, J. Gu, Y. Li, J. Wang, *Angew. Chem. Int. Ed.* **2019**, *58*, 587–591; *Angew. Chem.* **2019**, *131*, 597–601.
- [6] G. R. Kiel, S. C. Patel, P. W. Smith, D. S. Levine, T. D. Tilley, *J. Am. Chem. Soc.* **2017**, *139*, 18456–18459.
- [7] Examples of other expanded helicenes. a) S. Han, A. D. Bond, R. L. Disch, D. Holmes, J. M. Schulman, S. J. Teat, K. P. C. Vollhardt, G. D.

COMMUNICATION

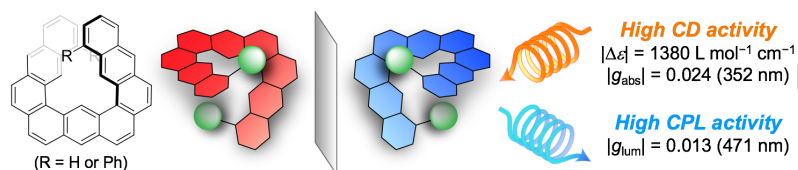
- Whitener, *Angew. Chem. Int. Ed.* **2002**, *41*, 3223–3227; *Angew. Chem.* **2002**, *114*, 3357–3361; b) S. Han, D. R. Anderson, A. D. Bond, H. V. Chu, R. L. Disch, D. Holmes, J. M. Schulman, S. J. Teat, K. P. C. Vollhardt, G. D. Whitener, *Angew. Chem. Int. Ed.* **2002**, *41*, 3227–3230; *Angew. Chem.* **2002**, *114*, 3361–3364; c) N. J. Schuster, D. W. Paley, S. Jockusch, F. Ng, M. L. Steigerwald, C. Nuckolls, *Angew. Chem. Int. Ed.* **2016**, *55*, 13519–13523; *Angew. Chem.* **2016**, *128*, 13717–13721; d) N. J. Schuster, R. H. Sánchez, D. Bukharina, N. A. Kotov, N. Berova, F. Ng, M. L. Steigerwald, C. Nuckolls, *J. Am. Chem. Soc.* **2018**, *140*, 6235–6239; e) J. Nejedlý, M. Šámal, J. Rybáček, M. Tobrmanová, F. Szydło, C. Coudret, M. Neumeier, J. Vacek, J. V. Chocholoušová, M. Buděšínský, D. Šaman, L. Bednářová, L. Sieger, I. G. Stará, I. Starý, *Angew. Chem. Int. Ed.* **2017**, *56*, 5839–5843; *Angew. Chem.* **2017**, *129*, 5933–5937.
- [8] Y. Nakakuki, T. Hirose, K. Matsuda, *J. Am. Chem. Soc.* **2018**, *140*, 15461–15469.
- [9] a) B. Valeur, M. N. Berberan-Santos, *Molecular Fluorescence: Principles and Applications*, 2nd ed., Wiley-VCH, Weinheim, **2012**, chap. 6; b) V. Gray, D. Dzebo, A. Lundin, J. Alborzpour, M. Abrahamsson, B. Albinsson, K. Moth-Poulsen, *J. Mater. Chem. C* **2015**, *3*, 11111–11121.
- [10] a) M. Yoshizawa, J. K. Klosterman, *Chem. Soc. Rev.* **2014**, *43*, 1885–1898; b) M. Nagaoka, E. Tsurumaki, M. Nishiuchi, T. Iwanaga, S. Toyota, *J. Org. Chem.* **2018**, *83*, 5784–5790; c) S. Toyota, M. Yoshikawa, T. Saibara, Y. Yokoyama, T. Komori, T. Iwanaga, *ChemPlusChem* **2019**, *84*, 643–654.
- [11] a) E. M. Sánchez-Carnerero, A. R. Agarrabeitia, F. Moreno, B. L. Maroto, G. Muller, M. J. Ortiz, S. de la Moya, *Chem. Eur. J.* **2015**, *21*, 13488–13500; b) H. Tanaka, Y. Inoue, T. Mori, *ChemPhotoChem* **2018**, *2*, 386–402; c) N. Chen, B. Yan, *Molecules* **2018**, *23*, 3376; d) Y. Sang, J. Han, T. Zhao, P. Duan, M. Liu, *Adv. Mater.* doi.org/10.1002/adma.201900110.
- [12] a) A. Fürstner, V. Mamane, *J. Org. Chem.* **2002**, *67*, 6264–6267; b) V. Mamane, P. Hannen, A. Fürstner, *Chem. Eur. J.* **2004**, *10*, 4556–4575.
- [13] J. Carreras, M. Patil, W. Thiel, M. Alcarazo, *J. Am. Chem. Soc.* **2012**, *134*, 16753–16758.
- [14] The low yield of cycloisomerization of **7c** to form **4c** was mainly attributed to the formation of an isomeric product.
- [15] B. V. Cheney, *J. Am. Chem. Soc.* **1968**, *90*, 5386–5390.
- [16] a) E. D. Becker, *High Resolution NMR: Theory and Chemical Applications*, 3rd ed. Academic Press, San Diego, **2000**, chap. 8.3; b) J. Brison, C. de Bakker, N. Defay, F. Geerts-Evrard, M.-J. Marchant, R. H. Martin, *Bull. Soc. Chim. Belg.* **1983**, *92*, 901–912.
- [17] D. Nori-shargh, S. Asadzadeh, F.-R. Ghanizadeh, F. Deyhimi, M. M. Amini, S. Jameh-Bozorghii, *THEOCHEM* **2005**, *717*, 41–51.
- [18] H. Tanaka, M. Ikenosako, Y. Kato, M. Fujiki, Y. Inoue, T. Mori, *Commun. Chem.* **2018**, *1*, 38.
- [19] a) O. E. Weigang, J. A. Turner, P. A. Trouard, *J. Chem. Phys.* **1966**, *45*, 1126–1134; b) M. Sapir, E. Vander Donckt, *Chem. Phys. Lett.* **1975**, *36*, 108–110.
- [20] Y. Yoshida, Y. Nakamura, H. Kishida, H. Hayama, Y. Nakano, H. Yamochi, G. Saito, *CrystEngComm* **2017**, *19*, 3626–3632.
- [21] T. M. Krygowski, M. K. Cyrański, *Chem. Rev.* **2001**, *101*, 1385–1419.
- [22] Z. Chen, C. S. Wannere, C. Corminboeuf, R. Puchta, P. v. R. Schleyer, *Chem. Rev.* **2005**, *105*, 3842–3888.
- [23] S. Toyota, T. Oki, M. Inoue, K. Wakamatsu, T. Iwanaga, *Chem. Lett.* **2015**, *44*, 978–980.
- [24] a) R. H. Martin, M. J. Marchant, *Tetrahedron* **1974**, *30*, 347–349; b) R. H. Janke, G. Haufe, E.-U. Würthwein, J. H. Borkent, *J. Am. Chem. Soc.* **1996**, *118*, 6031–6035; c) J. Barroso, J. L. Cabellos, S. Pan, F. Murillo, X. Zarate, M. A. Fernandez-Herrera, G. Merino, *Chem. Commun.* **2018**, *54*, 188–191.
- [25] Y. Zhu, X. Guo, Y. Li, J. Wang, *J. Am. Chem. Soc.* **2019**, *141*, 5511–5517.
- [26] A. Bedi, O. Gidron, *Acc. Chem. Res.* **2019**, *52*, 2482–2490.
- [27] S. Parsons, H. D. Flack, T. Wagner, *Acta Cryst.* **2013**, *B69*, 249–259.
- [28] Examples of other small organic molecules with high CPL activity. a) K. Nakamura, S. Furumi, M. Takeuchi, T. Shibuya, K. Tanaka, *J. Am. Chem. Soc.* **2014**, *136*, 5555–5558. (double azahelicene, $|g_{lum}| = 0.028$); b) S. Sato, A. Yoshii, S. Takahashi, S. Furumi, M. Takeuchi, H. Isobe, *Proc. Nat. Acad. Sci. USA* **2017**, *114*, 13097–13101 (chiral cylinder, 0.152); c) C. Schaack, L. Arrico, E. Sidler, M. Górecki, L. Di Bari, F. Diederich, *Chem. Eur. J.* **2019**, *25*, 8003–8007 (helicene, 0.025); d) J. Wang, G. Zhuang, M. Chen, D. Lu, Z. Li, Q. Huang, H. Jia, S. Cui, X. Shao, S. Yang, P. Du, *Angew. Chem. Int. Ed.* **2020**, *59*, 1619–1626; *Angew. Chem.* **2020**, *132*, 1636–1643 (anthracene macrocycle, ca. 0.1).
- [29] Y. Sawada, S. Furumi, A. Takai, M. Takeuchi, K. Noguchi, K. Tanaka, *J. Am. Chem. Soc.* **2012**, *134*, 4080–4083.
- [30] We also carried out the calculations of **4b** (Tables S5 and S7), and discussed the results in a similar manner to **4a**.
- [31] a) J. A. Schellman, *Chem. Rev.* **1975**, *75*, 323–331; b) F. S. Richardson, J. P. Riehl, *Chem. Rev.* **1977**, *77*, 773–792.

COMMUNICATION

Entry for the Table of Contents

Chiral Aromatic Chemistry

K. Fujise, E. Tsurumaki, G. Fukuhara, N. Hara, Y. Imai, S. Toyota*

Multiply fused anthracenes as helical polycyclic aromatic hydrocarbon motif for chiroptical performance enhancement

Helical expansion: A novel helical structure consisting of three fused anthracene units was constructed by cycloisomerization. Enantiomers of the diphenyl derivative exhibited excellent chiroptical performance in the circular dichroism spectra and the circularly polarized luminescence spectra as simple organic molecules.